arXiv:0712.2015v2 [astro-ph] 19 Mar 2008

A CELESTIAL GAMMA-RAY FOREGROUND DUE TO THE ALBEDO OF SMALL SOLAR SYSTEM BODIES AND A REMOTE PROBE OF THE INTERSTELLAR COSMIC RAY SPECTRUM

Igor V. Moskalenko[1]

Hansen Experimental Physics Laboratory, Stanford University, Stanford, CA 94305

Troy A. Porter

Santa Cruz Institute for Particle Physics, University of California, Santa Cruz, CA 95064

Seth W. Digel[1]

Stanford Linear Accelerator Center, 2575 Sand Hill Road, Menlo Park, CA 94025

Peter F. Michelson[1]

Department of Physics, Stanford University, Stanford, CA 94305

and

Jonathan F. Ormes

Department of Physics and Astronomy, University of Denver, Denver, CO 80208

Draft version March 19, 2008

ABSTRACT

We calculate the γ-ray albedo flux from cosmic-ray (CR) interactions with the solid rock and ice in Main Belt asteroids (MBAs), Jovian and Neptunian Trojan asteroids, and Kuiper Belt objects (KBOs) using the Moon as a template. We show that the γ-ray albedo for the Main Belt, Trojans, and Kuiper Belt strongly depends on the small-body size distribution of each system. Based on an analysis of the *Energetic Gamma Ray Experiment Telescope* (EGRET) data we infer that the diffuse emission from the MBAs, Trojans, and KBOs has an integrated flux of less than $\sim 6 \times 10^{-6}$ cm^{-2} s^{-1} (100–500 MeV), which corresponds to ~ 12 times the Lunar albedo, and may be detectable by the forthcoming *Gamma Ray Large Area Space Telescope* (GLAST). If detected by GLAST, it can provide unique direct information about the number of small bodies in each system that is difficult to assess by any other method. Additionally, the KBO albedo flux can be used to probe the spectrum of CR nuclei at close-to-interstellar conditions. The orbits of MBAs, Trojans, and KBOs are distributed near the ecliptic, which passes through the Galactic center and high Galactic latitudes. Therefore, the asteroid γ-ray albedo has to be taken into account when analyzing weak γ-ray sources close to the ecliptic, especially near the Galactic center and for signals at high Galactic latitudes, such as the extragalactic γ-ray emission. The asteroid albedo spectrum also exhibits a 511 keV line due to secondary positrons annihilating in the rock. This may be an important and previously unrecognized celestial foreground for the *INTErnational Gamma-Ray Astrophysics Laboratory* (INTEGRAL) observations of the Galactic 511 keV line emission including the direction of the Galactic center.

Subject headings: elementary particles — Kuiper Belt — minor planets, asteroids — Galaxy: bulge — cosmic rays — gamma-rays: theory

1. INTRODUCTION

The populations of small solar system bodies (SSSB) in the asteroid belt between Mars and Jupiter, Jovian and Neptunian Trojans, and in the Kuiper Belt beyond Neptune's orbit (often called also trans-Neptunian objects – TNOs) remain the least explored members of the solar system. A majority of the MBAs and KBOs have their orbits distributed near the ecliptic with a FWHM of the order of 10° in ecliptic latitude (Binzel et al. 1999; Brown 2001). The spatial and size distributions of these objects provides important information about the dynamical evolution of the solar system. Extending our knowledge of the size distribution of these objects below current sub-kilometer size limits of optical (e.g., Ivezić et al. 2001;

Wiegert et al. 2007) and infrared (e.g., Tedesco & Desert 2002; Yoshida et al. 2003) measurements would provide additional information on the accretion/collision and depletion processes that formed the populations of SSSBs[2]. In this paper we show that the CR-induced γ-ray albedo of these systems may be bright enough to be detected with a γ-ray telescope such as GLAST and/or INTEGRAL and/or Soft Gamma-ray Detector (SGD) aboard the NeXT satellite (Takahashi et al. 2006) (see our estimates below), and can allow us to probe the size distribution of SSSBs down to a few metres. Additionally, the γ-ray emission of these systems may comprise a "diffuse" γ-ray foreground that should be taken into account when evaluating the flux and spectra of γ-ray sources

---

[1] Also Kavli Institute for Particle Astrophysics and Cosmology, Stanford University, Stanford, CA 94309

[2] We note that Babich et al. (2007) have suggested a method to place constraints upon the mass, distance, and size distribution of TNOs using spectral distortions of the CMB.

near the ecliptic. Our preliminary results are presented in Moskalenko et al. (2008).

The Galactic center is a region crowded with γ-ray sources and is one of the preferred places to look for γ-ray signatures of dark matter (DM). An extensive literature on the subject exists, e.g., Bergström et al. (1998), Zaharijas & Hooper (2006), Finkbeiner & Weiner (2007), Hooper et al. (2008), Baltz et al. (2008); also references in these papers. The ecliptic crosses the Galactic equator near the Galactic center almost perpendicularly with inclination $\sim$86.5°, and underestimation of the SSSB albedo foreground may lead to errors in the analysis of weak or extended sources in this region.

The Galactic center region also harbors the enigmatic source of the 511 keV positron annihilation line observed by the *Oriented Scintillation Spectrometer Experiment* (OSSE) (e.g., Purcell et al. 1997) and INTEGRAL (e.g., Knödlseder et al. 2005; Weidenspointner et al. 2006). The distribution of the annihilation line does not match the distribution of any positron source candidate, e.g., pulsars, supernova remnants, binaries, radioactive isotopes, such as ^{26}Al, etc. A number of excellent discussions on the origin of this emission are available in the literature, ranging from positron focusing by the regular Galactic magnetic field to DM annihilation (Finkbeiner & Weiner 2007; Guessoum et al. 2005; Hooper et al. 2008; Jean et al. 2006; Prantzos 2006, and references therein). Our calculations (detailed below) indicate the SSSB CR-induced albedo spectrum should exhibit a 511 keV line due to secondary positrons annihilating in the rock. Since the target material (rock, ice) is solid, the line has to be very narrow. This emission produces a previously unrecognized celestial foreground to the 511 keV flux including the direction of the Galactic center.

At higher energies, above $\sim$30 MeV, regions at high Galactic latitudes are conventionally used to derive the level of the extragalactic γ-ray emission by comparing a model of the diffuse Galactic emission to the point-source-subtracted skymaps and extrapolating to zero model flux (e.g., Sreekumar et al. 1998; Strong et al. 2004). The remainder is assumed to represent the level of the isotropic, presumably extragalactic emission. However, recent studies have predicted another important foreground component with a broad distribution on the sky originating from the inverse Compton scattering of solar photons by CR electrons in the heliosphere (Moskalenko et al. 2006; Orlando & Strong 2007), which has to be included in the analysis of the diffuse emission. A reanalysis of the EGRET data revealed this broad component, in agreement with the predictions (Orlando et al. 2007). Since the ecliptic passes through high Galactic latitudes, the SSSB albedo flux also may need to be taken into account when analysing the weak extragalactic component.

2. SMALL SOLAR SYSTEM BODIES

The asteroid mass and size distributions are thought to be governed by collisional evolution and accretion. Collisions between asteroids give rise to a cascade of fragments, shifting mass toward smaller sizes, while slow accretion leads to the growth of the latter. The first comprehensive analytical description of such a collisional cascade is given by Dohnanyi (1969). Under the assumptions of scaling of the collisional response parameters and an upper cutoff in mass, the relaxed size and mass distributions approach power-laws:

$$dN = am^{-k}dm \qquad (1)$$
$$dN = br^{-n}dr, \qquad (2)$$

where m is the asteroid mass, r is the asteroid radius, and a, b, k, n are constants. These equilibrium distributions extend over all size and mass ranges of the population except near its high-mass end. The constants in eqs. (1), (2) are not independent. If all asteroids have the same density ρ, one obtains $n = 3k - 2$ and $b = 3a(4\pi\rho/3)^{1-k}$ (see eqs. [3], [4]). For a pure Dohnanyi cascade $k = 11/6$ and $n = 3.5$.

However, collisional response parameters are not size-independent, e.g., the energy per unit target mass delivered by the projectile required for catastrophic disruption of the target (the so-called critical specific energy) depends on the radius of the body, and the single power-laws (eqs. [1], [2]) break. Even though the sizes of asteroids generally can not be directly observed (except by a small number of asteroids studied by spacecraft flybys, by stellar occultation, or those well observed by radar) and are instead estimated using apparent magnitude, optical and infrared albedos, and distances, the information collected on a large sample of MBAs[3] seems to confirm that the real distribution departs from a single power law, at least for objects larger than a few kilometers. Smaller sizes are very difficult to detect, and one has bear in mind the observational bias of the incompleteness of the small (dim) asteroid sample. Though de-biasing can be attempted (e.g., Jedicke & Metcalfe 1998), a large ambiguity still remains.

Figure 1 shows the MBA size distributions as published in the literature and those used in this paper. For the MBAs larger than diameter $\mathcal{D}$ (km), Binzel et al. (1999) give $N(> \mathcal{D}) = 1.9 \times 10^6 \mathcal{D}^{-2.52}$ (the authors do not give the range of sizes, so we adopted a cut at $\mathcal{D} \sim 0.5$ km). Tedesco & Desert (2002) give $\log N(> \mathcal{D}) = (5.9324 \pm 0.0016) - (1.5021 \pm 0.045) \log \mathcal{D}$ for 0.2 km $< \mathcal{D} < 2$ km based on *Infrared Space Observatory* (ISO) observations. Using a sample of more than 6×10^4 MBAs to a limiting magnitude of $V \sim 21$, Jedicke & Metcalfe (1998) found a change in the slope of the cumulative distribution from –2.25 for 1 km $\lesssim \mathcal{D} \lesssim$ 10 km to –4.00 for 10 km $\lesssim \mathcal{D} \lesssim$ few 10s of km. Based on observations of $\sim$13000 MBAs by the Sloan Digital Sky Survey (SDSS), Ivezić et al. (2001) found that the cumulative size distribution resembles a broken power-law, $\propto \mathcal{D}^{-2.3}$ for 0.4 km $\lesssim r \lesssim 5$ km, and $\propto \mathcal{D}^{-4}$ for 5 km $\lesssim r \lesssim 40$ km, and is independent of the heliospheric distance. Finally, Tedesco et al. (2005) gives a fit to data between 1 km $\lesssim \mathcal{D} \lesssim 100$ km, $\log N(> \mathcal{D}) = 6.275 \pm 0.013 - (3.214 \pm 0.056) \log \mathcal{D} + (0.974 \pm 0.066) \log^2 \mathcal{D} - (0.182 \pm 0.022) \log^3 \mathcal{D}$, but extrapolation to smaller sizes is invalid. The size distribution below $\sim$1 km is essentially unexplored territory. One piece of evidence comes from the size distribution of ejecta blocks on 433 Eros. Based on the block distribution over a size range $0.1 – 150$ m, Cheng (2004) argued

---

[3] The Minor Planet Center supports a database for all observed SSSBs: http://www.cfa.harvard.edu/iau/mpc.html
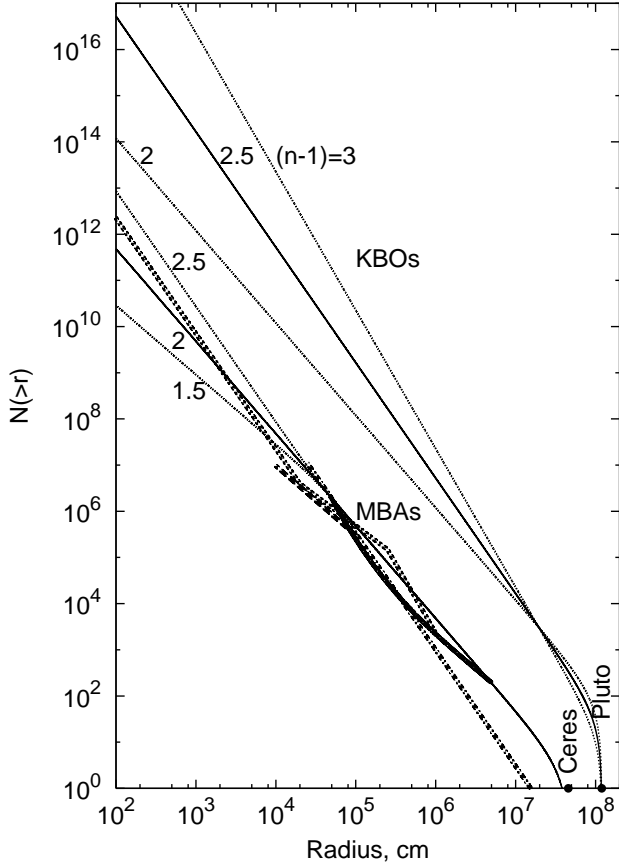
FIG. 1.— Cumulative size distribution $N(> r)$ of KBOs (upper set of lines) and MBAs (lower set of lines). Line coding: thick dash-dot line – Binzel et al. (1999), thick dashes – Tedesco & Desert (2002), thick solid – Tedesco et al. (2005), thick dots – parameterization proposed by Cheng (2004). Our parameterizations are shown by thin lines (solid, dotted) where the numbers show the *cumulative* power-law index $(n - 1)$ of a particular distribution. Thin solid lines are our adapted distributions: index 2.0 ($n = 3.0$) for MBAs, and 2.5 ($n = 3.5$) for KBOs. Thin dotted lines show the range discussed in the paper. See text for details.

that these data support a cumulative index 2.5 extrapolation down to sizes ∼1 m. Our distribution with a single cumulative index $(n - 1) = 2$ (thin solid line), detailed in the next Section, seems to match the global size distribution determined from various types of observations in the wide range of radii $10^2 - 10^7$ cm. We will use this distribution in our estimates of the MBA albedo, below.

The dynamical estimate of the total mass of the asteroid belt is about $(3.6 \pm 0.4) \times 10^{24}$ g (Krasinsky et al. 2002) or close to 5% of the mass of the Moon. The total mass is dominated by large bodies, while the γ-ray albedo is dominated by very small bodies. The largest MBA, 1 Ceres, comprises about 30% of the total mass of the asteroid belt alone. However, it does not provide a restriction on the size (and mass) distribution of small bodies. Current estimates indicate the total number of MBAs above 1 km in diameter is $(1.2 - 1.9) \times 10^6$ (Binzel et al. 1999; Tedesco & Desert 2002; Tedesco et al. 2005). Our adopted distribution with $n = 3$ gives a number near the upper end of this range, 1.92×10^6, while also putting the total number of MBAs with $r > 1$ m at $\sim 5 \times 10^{11}$ (Figure 1). To get an idea of how the MBA albedo flux

depends on the extrapolation to small radii $\mathcal{D} < 1$ km, we also consider broken power-law distributions with indices 2.5 and 3.5 below 1 km in diameter, retaining an index 3 for sizes larger than 1 km.

The densities of most MBAs lie in the range $1.0 - 3.5$ g cm^{-3} (Binzel et al. 1999) while the densities of particular asteroid classes can vary broadly, $1.23 - 1.40$ g cm^{-3} for carbonaceous, $2.65 - 2.75$ g cm^{-3} for silicate, and $4.75 - 5.82$ g cm^{-3} for metallic bodies (Krasinsky et al. 2002). We adopt an average density $\rho = 2$ g cm^{-3}.

Most MBAs have a semimajor axis between 2.1 and 3.3 AU with a low eccentricity orbit. In our estimates we assume an average circular orbit with radius $\ell \sim 2.7$ AU.

The Jovian Trojan populations of asteroids are collections of bodies in the same orbit as Jupiter (semimajor axis $\ell \sim 5.2$ AU) located at the L_4 and L_5 Lagrange points of the Jupiter-Sun system. The Trojans are thus concentrated in two regions rather than distributed over the entire ecliptic as for the MBAs. The total mass of the Jovian Trojans is estimated to be $\sim 10^{-4}$ $M_\oplus$ where $M_\oplus$ is the mass of the Earth with a differential power-law index $n \simeq 3$ in the size range 2 km to 20 km (Jewitt et al. 2000; Yoshida & Nakamura 2005), similar to MBAs, giving a number of objects ≥ 1 km in diameter $\sim 1.3 \times 10^6$ (Jewitt et al. 2000). The combined mass of these objects is approximately the same as for the MBAs. The number of objects ≥ 1 km in diameter and the power-law index $n \simeq 3$ makes their size distribution very similar to that of MBAs.

The mass density of SSSBs in this group varies significantly: estimates for the binary Trojan 617 Patroclus are less than water ice $\rho = 0.8^{+0.2}_{-0.1}$ g cm^{-3} (Marchis et al. 2006), as are those for other Trojan binaries $\rho \sim 0.6 - 0.8$ g cm^{-3} (Mann et al. 2007), while 624 Hektor is somewhat denser $\rho = 2.48^{+0.292}_{-0.080}$ g cm^{-3} (Lacerda & Jewitt 2007). In our calculations we adopt an average density $\rho = 1$ g cm^{-3} as a compromise between these bounds.

We also consider icy bodies and comets in the Kuiper Belt (for a review see Luu & Jewitt 2002) and the conjoining innermost part of the Oort Cloud[4], but call them all KBOs for simplicity. The KBOs are not uniformly distributed, with at least three dynamically distinct populations identified: the Classical Disk, the Scattered Disk with large eccentricities and inclinations, and "Plutinos" around the 3:2 mean motion resonance with Neptune at 39.4 AU. Kuiper Belt Objects are distributed between $30 - 100$ AU (Backman et al. 1995, and references therein) with surface number density $\sigma(\ell) = A\ell^{-\alpha}$ (Backman et al. 1995; Jewitt & Luu 1995), where A is a constant determined in eq. (11), and $\alpha = 2$. The total mass is estimated to be in the range ∼0.01–0.3 $M_\oplus$, while the most often used value is ∼0.1 $M_\oplus$ (Luu & Jewitt 2002). The density of small icy bodies and comets is ∼0.5 g cm^{-3} (Asphaug & Benz 1994; Solem 1994).

The KBO size distribution is much more difficult to determine because of their dimness. It is widely believed that the TNOs are dynamically related to the Centaurs

[4] The Oort Cloud of comets (e.g., Stern 2003) is thought to occupy a vast space between 50 and 50000 AU from the Sun and also contributes to the celestial γ-ray foreground. However, its exact mass and distribution are poorly constrained. We are planning to investigate limits on the albedo of the Oort Cloud in a forthcoming paper.

(planetesimals distributed between Jupiter and Neptune that are in crossing orbits of the giant gas planets), and to the Jupiter-family group of ecliptic comets that may be objects that were knocked inwards from the Kuiper belt. The KBO size distribution is determined by very indirect methods such as measuring the sizes of the nuclei of the ecliptic comets (and making assumptions on how they evolve during their repeated passages through the inner solar system), and Centaurs, as well as impact craters on the Galilean satellites of Jupiter. The estimates of the size distribution for the cometary nuclei range from $n = 2.6$ to 3.7 in the range $r \sim 1-10$ km, for KBOs – 3.7–4.45 ($r > 20$ km), and for Centaurs – 3.7–4.0 (an appropriate discussion can be found, e.g., in Bernstein et al. 2004, Toth 2005, Tancredi et al. 2006, and references therein). If the index is ≥ 4.0, the mass of the total population is dominated by the smallest bodies. However, there are some reasons to believe that the size distribution begins to flatten well above 1 km in size. Collisional evolution simulations (Kenyon & Bromley 2004) show that the size distribution is a power law with index ~ 4.5 for large bodies ($r \gtrsim 10 - 100$ km) and $\sim 3.5 - 4$ for small bodies ($r \lesssim 0.1 - 1$ km) for a wide range of bulk properties, initial masses, and orbital parameters. Adopting a conservative value of $n = 3.5$, we obtain the total number of comets ($\mathcal{D} > 1$ km) at $\sim 9 \times 10^9$, which is in agreement with other estimates (e.g., Stern 2003).

There are also large populations of Centaurs $N(\mathcal{D} > 1$ km$) \sim 10^8$ (Sheppard 2005) between the orbits of Jupiter and Neptune, and Neptunian Trojans at the L_4 and L_5 points of the Neptune-Sun system. The number of large Neptunian Trojans ($\mathcal{D} > 80$ km) outnumbers the number of large Jovian Trojans by a factor ~ 10 (Sheppard & Trujillo 2006). Their power-law index may be close to that of the KBOs $n \sim 3.5$ making their γ-ray albedo essentially brighter than MBAs and Jovian Trojans at the same distance. While Centaurs are scattered between Jupiter and Neptune, the positions of Neptunian Trojans are well known so that the detection of a γ-ray albedo signal may be simplified.

3. CALCULATIONS

We use the Lunar albedo spectrum as an approximation of the SSSB albedo for two main reasons: (i) the Moon is a solid body in which the CR cascade in the rock develops similarly, and (ii) its proximity to the Earth allows it to be easily detectable by γ-ray telescopes. The spectrum of γ-rays from the Moon has been calculated recently (Moskalenko & Porter 2007a,b) using the GEANT4 Monte Carlo framework to simulate the CR cascade development in a Lunar rock target (regolith). It has been shown that the Lunar albedo spectrum is very steep with an effective cutoff around 3–4 GeV in agreement with observations (Thompson et al. 1997). The central part of the disk of the Moon has an even steeper spectrum with an effective cutoff at $\sim$600 MeV. The emission above $\sim$10 MeV is thus dominated by the thin rim where CR particles interact close-to tangentially with the surface and the high-energy secondary γ-rays shower out of the Moon toward the observer. In contrast to other astrophysical sources, the albedo spectrum of the Moon is well understood, including its absolute normalization; this makes it a useful template for estimations of the CR-induced albedo of SSSBs without

an atmosphere. Since the Moon functions as a standard (γ-ray) candle, in our estimates we use the flux of the Moon as our standard and introduce the term "Lunar albedo flux units."

If the SSSB size distribution dN/dr is known, it can be directly substituted into eq. (6) to estimate the γ-ray albedo flux. Below, we derive this albedo flux assuming that the size distribution for a single SSSB population is a simple power law where the normalization has to be obtained from the total mass of the system.

Let the SSSB mass distribution have the form given by eq. (1), which can be rewritten as a size distribution (cf. eq. [2])

$$\frac{dN}{dr} = \frac{dN}{dm}\frac{dm}{dr} = 4\pi\rho r^2 \frac{dN}{dm}, \qquad (3)$$

where ρ is the average density of the SSSB target. Assuming that all SSSBs have a spherical shape, $m = (4\pi/3)\rho r^3$, we get

$$\frac{dN}{dr} = 3a\left(\frac{4\pi}{3}\rho\right)^{1-k} r^{2-3k}. \qquad (4)$$

The normalization for a is obtained from

$$\int_{m_0}^{m_1} m\frac{dN}{dm}dm = fM_{\text{Moon}}, \qquad (5)$$

where m_0 and m_1 are the lower and upper SSSB masses, respectively, and fM_{Moon} is the total mass of the SSSB emitting population considered as a fraction f of the Moon's mass ($f = 0.05$ for MBAs, $f = 0.1 M_\oplus/M_{\text{Moon}} \approx 8.13$ for KBOs). The flux of γ-rays from such an ensemble of bodies with size distribution dN/dr is then

$$F = F_{\text{Moon}}\left(\frac{D_{\text{Moon}}}{d}\right)^2 \int_{r_0}^{r_1} \frac{dN}{dr}\frac{r}{R_{\text{Moon}}}dr \qquad (6)$$

$$= \frac{F_{\text{Moon}}}{R_{\text{Moon}}}\left(\frac{D_{\text{Moon}}}{d}\right)^2 \left(\frac{4\pi}{3}\rho\right)^{1-k} 3a \int_{r_0}^{r_1} r^{3-3k}dr$$

where

$$\int_{r_0}^{r_1} r^{3-3k}dr = \begin{cases} \frac{1}{4-3k}\left(r_1^{4-3k} - r_0^{4-3k}\right), & k \neq 4/3 \\ \ln(r_1/r_0), & k = 4/3 \end{cases}$$

$$a = fM_{\text{Moon}} \begin{cases} \left(\frac{4\pi}{3}\rho\right)^{k-2} \frac{2-k}{r_1^{6-3k} - r_0^{6-3k}}, & k \neq 2 \\ \frac{1}{3}\ln^{-1}(r_1/r_0), & k = 2 \end{cases}$$

Here F_{Moon} is the Lunar rim albedo flux for the same incident spectrum of CR particles, $R_{\text{Moon}} = 1.7382 \times 10^8$ cm is the Lunar radius, $D_{\text{Moon}} \simeq 0.0025$ AU is the Earth-Moon distance, d is the distance (in AU) of the SSSB population from Earth, and r_0 and r_1 are the sizes corresponding to the masses m_0 and m_1.

The factor r/R_{Moon} in eq. (6) comes from the fact that the albedo of SSSBs is dominated by the emission from the rim. The rim and the disk albedo fluxes of the Moon are about equal at low energies (Figure 2), with the rim albedo flux considerably dominating above 10 MeV (Moskalenko & Porter 2007b). Since the rim albedo flux scales $\propto r$, and the inner part of the disk $\propto r^2$, as the size of the emitting body decreases it is the rim which produces most of the albedo photons for SSSBs.

Assuming $k \neq 4/3, 2$, after some rearrangement we obtain

$$F(\ell, \theta) = \frac{3}{2\pi} f F_{\mathrm{Moon}} R_{\mathrm{Moon}}^2 \frac{\rho_{\mathrm{Moon}}}{\rho} \left[\frac{D_{\mathrm{Moon}}}{d(\ell, \theta)} \right]^2 G(r_1, r_0; k),$$
(7)

$$G(r_1, r_0; k) = \frac{1}{r_1^2} \left[\frac{2-k}{4-3k} \right] \left[\frac{1-(r_0/r_1)^{4-3k}}{1-(r_0/r_1)^{6-3k}} \right],$$
(8)

where $\rho_{\mathrm{Moon}} = 3.3$ g cm^{-3} is the mean density of the Moon,

$$d(\ell, \theta) = \cos\theta + \left(\ell^2 - \sin^2\theta \right)^{1/2},$$
(9)

ℓ (AU) is the radius of the orbit of the SSSB population (for MBAs, $\ell = 2.7$ AU; for KBOs, see below), θ is the angle between the line of sight (in the ecliptic) and the direction to the Sun, and we divided by 2π to obtain the flux per radian. The total flux integrated over θ is

$$F_{\mathrm{tot}} = \int_0^{2\pi} F(\ell, \theta) d\theta.$$
(10)

For the case of the KBOs distributed between $\ell = 30$ and 100 AU, an additional integration over ℓ is required

$$F_{\mathrm{tot}}^{\mathrm{K}} = \int_0^{2\pi} d\theta \int_{30}^{100} F(\ell, \theta) \sigma(\ell) \ell d\ell,$$
(11)

where $\sigma(\ell) = A\ell^{-2}$ and $A = -f/\ln 0.3$. These formulae provide fluxes integrated over ecliptic latitude.

For the case of MBAs, our adopted differential size distribution is a broken power law with index $n_1 = 3k_1 - 2$ for $r > r_b$ and $n_2 = 3k_2 - 2$ for $r < r_b$:

$$\frac{dN}{dr} = 3f M_{\mathrm{Moon}} \left(\frac{4\pi}{3}\rho \right)^{-1}$$
(12)

$$\times \frac{2-k_1}{r_1^{6-3k_1} - r_0^{6-3k_1}} \begin{cases} r^{2-3k_1}, & r \geq r_b \\ r_b^{2-3k_1} \left(\frac{r}{r_b} \right)^{2-3k_2}, & r < r_b \end{cases}$$

where $r_b = 0.5 \times 10^5$ cm, and we assume $2 < n_{1,2} < 4$. This can be inserted into eq. (6) to derive corresponding expressions for the flux from such a population of SSSBs.

We can see that the observed albedo flux gives direct information on the integral $\int dr\, r\, (dN/dr)$, eq. (6), which can be used to constrain the effective average radius of the emitting bodies $\langle r \rangle$ and their total number in the system. Additionally, if the size distribution is a single power law, the observed albedo flux can provide us with information about the power-law index. As can be seen from eq. (8), the function $G(r_1, r_0; k)$ is a steep function of k. For $k < 4/3$, the expression in the last square brackets (eq. [8]) is ~ 1 since $r_1 \gg r_0$ and $G \approx r_1^{-2}(2-k)/(4-3k)$. For $k > 2$, eq. (8) becomes $G \approx r_0^{-2}(2-k)/(4-3k)$. In the intermediate region $4/3 < k < 2$, G quickly increases with k. For the distribution of radii we consider the corresponding range for the size distribution index is $n = 2.5 - 3.5$ for MBAs and 3.0–4.0 for KBOs. This translates into an index, k, for the mass distribution in the range 1.5–2.0. In this range $G(r_1, r_0; k)$ changes by $3 - 5$ orders of magnitude depending mostly on the assumed value of r_0. This allows a determination of k assuming the average density

of the asteroid rocks is known. The function G also contains a dependence on r_1, the radius of the largest body. For the MBAs, we use Ceres, $r_1 = 4.565 \times 10^7$ cm, and for the KBOs we use 134340 Pluto, $r_1 = 1.195 \times 10^8$ cm, but the exact value of r_1 does not change the size distribution significantly and does not affect our conclusions. Figure 1 shows the adopted size distributions of MBAs and KBOs which agree well with those given in the literature.

The question of where most of the heliospheric modulation occurs is important for the determination of the CR flux at an arbitrary distance from the Sun. The recent crossing of the heliospheric termination shock by the Voyager 1 spacecraft at ~ 94 AU (Stone et al. 2005), currently at ~ 104 AU, while Voyager 2 is still inside the termination shock, allows unique studies of the spectra of CR particles on both sides of the shock. Low-energy CR detectors on board the spacecraft indicate that the particle spectra are significantly different, supporting the conclusion that a considerable modulation of the CRs occurs near the termination shock. On the other hand, most of the albedo emission discussed in this paper is produced by CR particles with energies >1 GeV; their flux does not change significantly from local interstellar space down to ~ 40 AU, as indicated by current heliospheric models (e.g., Langner et al. 2006).

The Lunar albedo flux, F_{Moon}, is calculated using the procedure described in Moskalenko & Porter (2007b). To calculate the Lunar albedo at an arbitrary modulation level, we use the local interstellar (LIS) spectra of CR protons, helium, and positrons, as fitted to the numerical results of the GALPROP propagation model (Ptuskin et al. 2006, Table 1, reacceleration and plain diffusion models) as described in Moskalenko & Porter (2007b, eq. (2) with parameters listed in Table 1)[5]. The CR particle flux at an arbitrary phase of solar activity can then be estimated using the force-field approximation (Gleeson & Axford 1968):

$$\frac{dJ_p(E_k)}{dE_k} = \frac{dJ_p^\infty(E_k + \Phi Z/A)}{dE_k} \frac{E^2 - M^2}{(E + \Phi Z/A)^2 - M^2},$$
(13)

where dJ_p^∞/dE_k is the LIS spectrum of the CR species, E_k is the kinetic energy per nucleon, E is the total energy per nucleon, Φ is the modulation potential, Z and A are the nuclear charge and atomic number correspondingly, and M is the nucleon mass. The modulation potential $\Phi(\ell)$ at an arbitrary distance ℓ from the Sun can be calculated using the expressions derived in Moskalenko et al. (2006), their eqs. (7), (8).

Figure 2 shows the Lunar albedo spectrum for different modulation potentials $\Phi = 0, 500, 1500$ MV. The no modulation case ($\Phi = 0$) corresponds to the upper limit of the KBO albedo, with moderate modulation ($\Phi = 500$ MV) corresponding to the MBA albedo. The difference in brightness below ~ 1 GeV due to the incident CR flux only (no modulation vs. moderate modulation) is as large as a factor of ~ 2–3. Also shown are the components of the albedo spectrum (center, rim) for $\Phi = 1500$ MV.

Figure 3 shows the albedo spectrum of the Moon as if

---

[5] The parameterization constants for CR positrons, not given in Table 1 of Moskalenko & Porter (2007b), are: $J_0 = 44.8143$, $a_1 = 1$, $b_1 = 0.594634$, $c_1 = -9.14888$, $a_2 = -605.291$, $b_2 = 1.53611$, $c_2 = -7.27809$, $a_3 = 1.18135$, $b_3 = 0.365787$, $c_3 = -3.51576$.
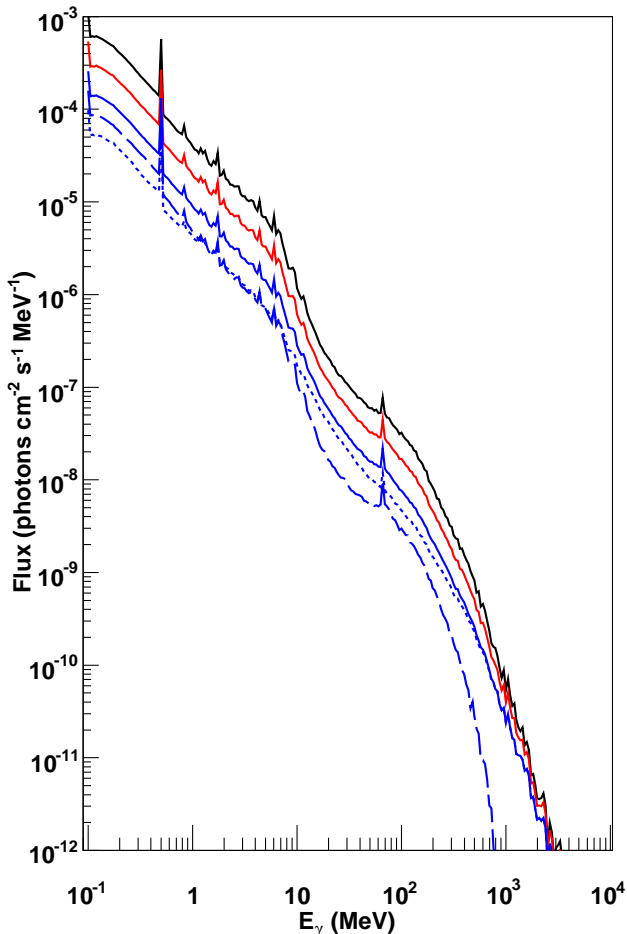
FIG. 2.— Calculated γ-ray albedo spectrum for CR nuclei inter-actions in the Moon rock Moskalenko & Porter (2007b) for selected modulation potentials. Line colouring: black, no modulation; red, $\Phi = 500$ MV; blue, $\Phi = 1500$ MV. Dashed and dotted lines show the albedo of the disk and the rim correspondingly for the case of $\Phi = 1500$ MV.

FIG. 3.— Calculated γ-ray albedo spectrum of a Moon-sized body at the Lunar distance composed of moon rock (black), iron ($\times 10$, blue), or water ice ($\times 0.1$, red). Line-styles: solid, no modulation; long-dashed, $\Phi = 1500$ MV.

the Lunar surface was made of different materials: water ice (multiplied by a factor of 0.1), regolith, and iron (mul-tiplied by a factor of 10). The plot shows the albedo spec-tra for two limiting cases, no solar modulation ($\Phi = 0$) and solar maximum conditions at 1 AU ($\Phi = 1500$ MV). The low-energy parts of the spectra (<10 MeV) from different materials are considerably different and the nu-clear emission lines can be used to distinguish between the materials. The high-energy parts are essentially fea-tureless and have similar shape. The flux between iron and water ice changes by a factor of ~ 2 above 100 MeV with the latter producing the larger flux. Above ~ 100 MeV the regolith albedo approaches the water ice albedo.

The 511 keV line in Figures 2 and 3 is due to the an-nihilation of positrons produced by CR cascades in the solid target (iron, regolith, ice). In Figure 2, the albedo spectrum also includes the contribution by CR positrons in the Lunar rock target (see below). Since the rock is solid, secondary positrons quickly thermalize and pro-duce a narrow annihilation line. Its width is determined
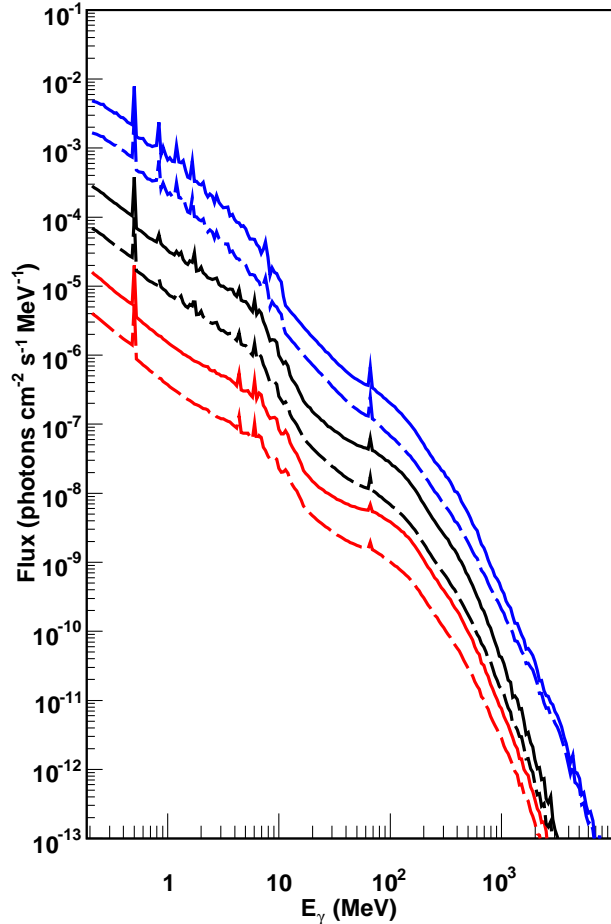
by the energy bin size adopted in the simulation.

Figure 4 shows the components of the albedo spec-trum (Figure 2) below 20 MeV. The thick solid lines are the total albedo flux due to the CR proton, helium, and positron interactions with regolith for no modulation (upper, red) and modulation level 1500 MV (lower, blue). The thin solid lines show the albedo spectrum due to CR positron interactions with regolith for the same cases of no modulation (upper, red) and modulation level 1500 MV (lower, blue). The dashed and dotted lines show the components of the CR positron induced γ-rays, from the center and the rim, correspondingly.

4. ANALYSIS OF THE EGRET DATA

The EGRET instrument on the Compton Gamma-Ray Observatory (1991–2000) surveyed the sky in the range >30 MeV and here we use the EGRET data together with the information in the Third EGRET Source Cata-log (3EG, Hartman et al. 1999) to set limits on the signal from the SSSBs. Challenges to detecting diffuse emission associated with the ecliptic plane include the brightness of the Galactic diffuse emission (e.g., Hunter et al. 1997),
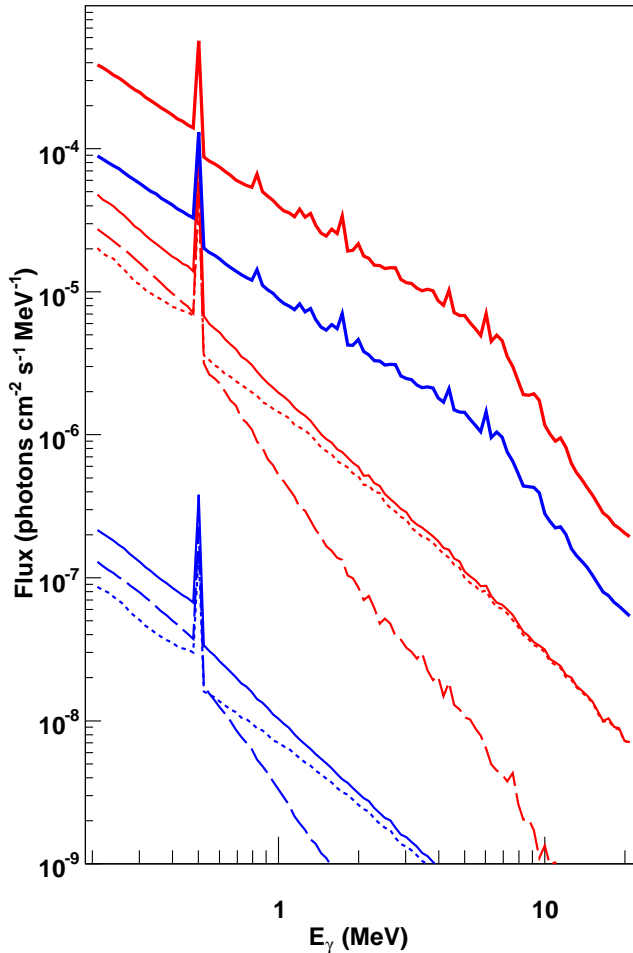
FIG. 4.— Calculated γ-ray albedo spectrum showing components below 20 MeV for no modulation (red) and modulation level 1500 MV (blue). Line-styles: long dash: positron induced γ-rays from center; short dash: CR positron induced γ-rays from rim; thin solid: total CR positron induced γ-rays; thick solid: total γ-ray emission from CR positrons and nucleons.
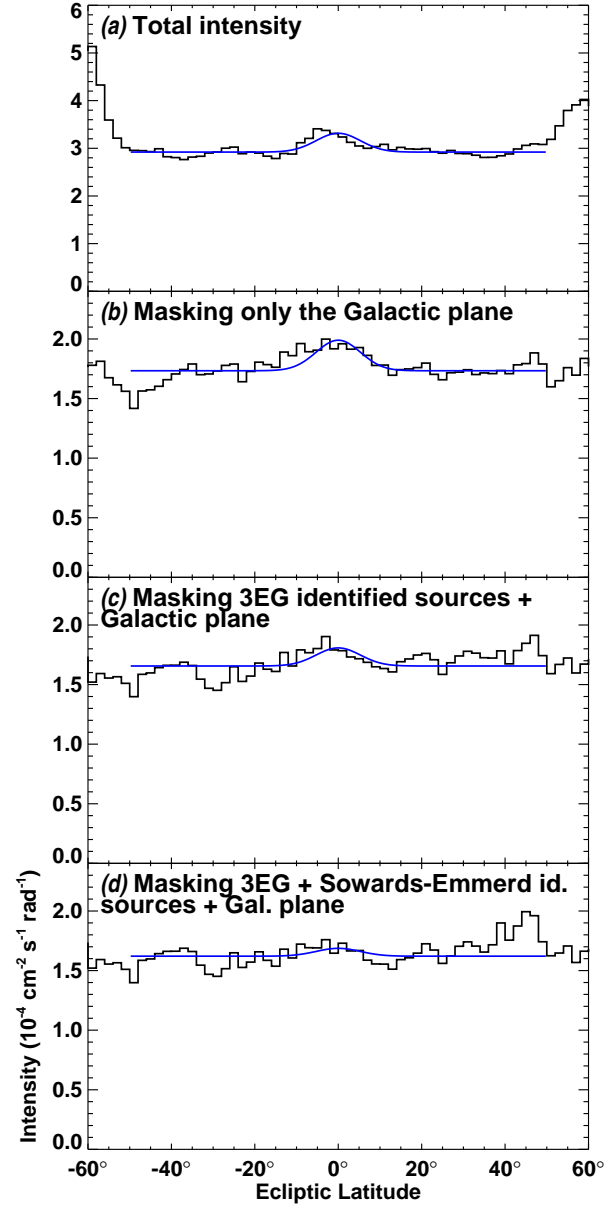

FIG. 5.— Profiles of γ-ray intensity with β derived from EGRET data as described in the text. The energy range is 100–500 MeV and the profiles have been averaged over all ecliptic longitudes. (a) Profile derived with no masking of Galactic diffuse emission or γ-ray point sources. (b) Profile with the Galactic plane ($|b| < 10°$ for $|l| > 90°$ and $|b| < 20°$ for $|l| < 90°$) excluded. (c) Profile with the identified 3EG sources (Hartman et al. 1999) and the Galactic plane excluded. (d) Profile with the identified 3EG sources plus the further blazar identifications proposed by Sowards-Emmerd (2003, 2004) excluded. Overlaid on each profile is the best-fitting gaussian (12.5° FWHM, centered on $\beta = 0$) plus a constant, fit for the region $|\beta| < 50°$. This approximates the distribution of albedo γ-ray emission expected for the the KBO.

the presence of bright point sources, the limited angular resolution and photon statistics of the EGRET data, and potential large-scale artifacts in the exposure maps owing to ageing of the spark chamber gas.

We made maps of the EGRET data in ecliptic coordinates for Cycles 1–4 of the mission, during which most of the EGRET exposure was obtained. The event data, after standard cuts on zenith angle and inclination angle (30°), were binned on a photon-by-photon basis in ecliptic coordinates. The exposure maps for each EGRET viewing period were transformed into ecliptic coordinates and added together and intensity maps were calculated from the photon and exposure maps.

In order to limit contributions from Galactic diffuse emission to any possible enhancement of diffuse intensity at low ecliptic latitudes, the region $|b| < 20°$ for $|l| < 90°$ and $|b| < 10°$ for $|l| > 90°$ was masked out in the analysis. We also removed regions 12° in diameter around the position of each identified source in the 3EG

catalog (designation other than "u" in the 3EG catalog).

Figure 5 presents the profile of γ-ray intensity in the 100–500 MeV range over ecliptic longitude. This range was chosen as having the brightest expected albedo emission in the energy range of EGRET. As described in the

TABLE 1. DIFFUSE INTENSITY AROUND THE ECLIPTIC (100–500 MeV)

Set of cuts in Figure 5	$\|\beta\| < 15°$ Flux, cm^{-2} s^{-1}	Stat. error	Fitted flux, cm^{-2} s^{-1}	Stat. error
a	1.006×10^{-5}	5.5×10^{-7}	9.16×10^{-6}	3.5×10^{-7}
b	7.95×10^{-6}	5.8×10^{-7}	5.95×10^{-6}	3.7×10^{-7}
c	3.59×10^{-6}	6.7×10^{-7}	3.53×10^{-6}	4.4×10^{-7}
d	1.1×10^{-7}	7.4×10^{-7}	1.52×10^{-6}	5.1×10^{-7}

caption, a sequence of profiles is shown for different combinations of the masks described above. In the last profile (Figure 5d), the 3EG sources subsequently identified by Sowards-Emmerd (2003, 2004) as likely to be blazars were included with the sources identified in the 3EG catalog in defining the mask. We did not mask out unidentified point sources because of the possibility that some of them may have represented detections of the γ-ray albedo from the Trojan groups, which move collectively, or fluctuations in the SSSB γ-ray albedo at low ecliptic latitudes.

In order to estimate the possible "excess" diffuse flux from MBAs, Trojans, and KBOs we calculated the integrated fluxes for ecliptic latitudes $|\beta| < 15°$ and all ecliptic longitudes (Table 1, "Flux" column). In order to increase the sensitivity, and to search for a diffuse signal that is centered on the ecliptic the table also includes fluxes for the best-fitting Gaussian centered on $\beta = 0°$ and having FWHM width 12.5° ("Fitted flux" column), the approximate extent of the Kuiper Belt (Brown 2001). The fits included a constant term to account for Galactic and extragalactic diffuse emission; profiles of the fits are included in Figure 5. The effective PSF for EGRET in the 100–500 MeV range for the expected spectrum of the albedo emission is approximately 4° FWHM, which would not appreciably broaden the apparent distribution of γ-ray intensity. In any case, the assumption of a single Gaussian profile is an approximation; the contribution from MBAs should result in an additional somewhat narrower but fainter component to the diffuse emission around the ecliptic.

Gamma-ray emission associated with the Moon and Sun also contributes to the intensity of the sky at low ecliptic latitudes. The Moon is always within about 5° of the ecliptic and the profiles shown in Figure 5 undoubtedly include lunar albedo γ-ray emission, at a level of $\sim 5 \times 10^{-7}$ cm^{-2} s^{-1} (Moskalenko & Porter 2007b). As described by Moskalenko et al. (2006) the solar radiation field is a fairly bright and diffuse γ-ray source from inverse Compton scattering of CR electrons. The solar inverse Compton emission is brightest in the ecliptic plane but of course depends on solar elongation angle. The precise contribution to the diffuse intensity at low ecliptic latitudes is difficult to estimate. The Sun was in the field of view of EGRET for only a small fraction of the observing time and the contribution to the total flux should have been less than that of the Moon.

After the bright diffuse emission and identified point sources are masked from the EGRET data, no strong excess of diffuse emission is apparent at low ecliptic latitudes in Figure 5. The integrated fluxes are formally significant for the case where the Galactic plane and all sources identified in the 3EG catalog are masked out (Ta-

ble 1, Figure 5c), but the systematic uncertainties are comparable to the measurement. This is suggested by the effect on the integrated flux from masking out several more sources that Sowards-Emmerd (2003, 2004) identified as blazars (Figure 5d). The overall average exposure does not change appreciably as a result of the additional masking but the fit flux decreased by more than 50% (Table 1).

Based on our analysis of the EGRET data we infer that the diffuse emission from MBAs, Trojans, and KBOs has an integrated flux of less than $\sim 6 \times 10^{-6}$ cm^{-2} s^{-1} (100–500 MeV), as derived from the set of cuts b, which corresponds to ~ 12 Lunar albedo flux units.

5. DISCUSSION AND CONCLUSION

The albedo γ-ray flux from MBAs can be calculated using eqs. (7)–(11) and Figures 2, 3 where we assume that their surface material is regolith. We use the following parameters: $\rho = 2$ g cm^{-3} for the MBA average density, $r_1 = 4.565 \times 10^7$ cm for the radius of Ceres, $r_0 = 100$ cm for the smallest radius of an asteroid that is still an opaque target for incident CR particles. The central grammage in this case ($r_0 = 100$ cm) is ~ 400 g cm^{-2}. Since the composition of the MBAs (and other SSSB populations) is mainly oxygen, this corresponds to ~ 5 interaction lengths which is sufficient for the hadronic cascade to fully develop at the CR energies we consider. With these parameters, the total MBA albedo flux is $\mathcal{X} = F_{\text{tot}}/F_{\text{Moon}} = 0.05, 0.67, 12$ for extrapolation to small sizes with indices $n = 2.5, 3.0, 3.5$ (see Figure 1), correspondingly.

Similarly, for the Jovian Trojan asteroids we can estimate the γ-ray flux assuming the same size distribution as for MBAs, but with $\ell \sim 5.2$ AU, and $r_0 = 200$ cm (which gives the same central grammage for $\rho = 1$ g cm^{-3}). We obtain $\mathcal{X} = F_{\text{tot}}/F_{\text{Moon}} = 0.01, 0.07, 0.8$ (averaged over their orbit) for a similar extrapolation to small sizes with indices $n = 2.5, 3.0, 3.5$. For the closest (4.2 AU) and the farthest (6.2 AU) distances to Earth, the fluxes will be 0.01, 0.1, 1.2 and 0.006, 0.05, 0.5, correspondingly.

The KBO size distribution is known very approximately. The second largest object of the Kuiper Belt after 136199 Eris is Pluto $r_1 = 1.195 \times 10^8$ cm, while the majority of the KBOs are icy rocks and comets with $\rho = 0.5$ g cm^{-3}. To keep the same central grammage of the smallest body ~ 400 g cm^{-2} we have to use a larger minimum radius, $r_0 = 400$ cm, than for the MBAs. The incident spectrum of CR particles at >30 AU approaches the LIS spectrum which results in a factor of ~ 2 increase below ~ 1 GeV of the albedo flux compared to the same body at 1 AU (Figure 2). For these parameters, the total Kuiper Belt albedo flux is $\mathcal{X}^{\text{K}} = F_{\text{tot}}^{\text{K}}/F_{\text{Moon}} = 0.2, 34,$

1168 for $n = 3.0$, 3.5, 3.9, correspondingly. The removal of Eris and Pluto ($\sim 0.005 M_{\oplus}$ combined) from the Kuiper Belt and using Charon instead, $r_1 = 6 \times 10^7$ cm, results in the flux increase: $\mathcal{X}^{\rm K} = F_{\rm tot}^{\rm K}/F_{\rm Moon} = 0.35$, 46, 1222 for the same values of n. However, this change is simply the result of anchoring the power-law size distribution to a large body.

Our estimates show that the albedo of MBAs and KBOs could account for the EGRET upper limit of the flux from the ecliptic. For the adopted size distributions of SSSBs ($n = 3.0$ for MBAs and $n = 3.5$ for KBOs), the KBO albedo is essentially brighter. However, if the MBA size distribution is somewhat steeper than our adopted index of $n = 3.0$, e.g., as for the distribution proposed by Cheng (2004), it can account for the total albedo flux from the ecliptic. The SSSB γ-ray albedo, especially of the collectively moving Trojan groups, might be responsible for some fraction of the EGRET unidentified point sources at low ecliptic latitudes.

A possible way to distinguish the albedo emission of MBAs and KBOs is to study the emission as a function of solar elongation angle. In the antisolar direction, $\theta \approx 180°$, the direction in which the Main Belt is closest to the Earth (~ 1.7 AU), the flux is predicted to be as much as ~ 5 times that in the solar direction, $\theta \approx 0°$. On the other hand, the brightness of the Kuiper Belt is only weakly dependent on the elongation angle because it is much further away. The positions of the Trojans on the sky are known, being determined relative to their respective planet (Jupiter, Neptune), making them easier to detect.

The detection of the CR-induced γ-ray albedo of MBAs, Trojans, and the KBOs by γ-ray instruments is possible. At higher energies $\gtrsim 1$ GeV where the γ-ray albedo flux is steady and does not depend on the solar modulation, it can serve as a normalization point to the cumulative brightness of all MBAs plus KBOs. At lower energies $\lesssim 1$ GeV, the component of the albedo which is independent of elongation, the KBO albedo, will tell us directly about the LIS spectrum of CRs. Therefore, the observations of the albedo flux can provide us with valuable information about the size distributions of SSSBs in both regions, while the shape of the albedo spectrum can tell us about the LIS spectra of CR protons and helium at high energies. In turn, a detection of the MBA and KBO albedo at MeV-GeV energies will enable us to normalize properly the cumulative albedo spectrum and make a prediction for the intensity of the 511 keV line.

A conservative estimate of the 511 keV line flux from SSSBs can be made using the upper limit derived in Section 4. The total flux of 511 keV photons from the Moon is $F_{\rm Moon}^{511} \approx 10^{-3}\Delta E \approx 2.4 \times 10^{-5}$ photons cm^{-2} s^{-1} (Figure 2, $\Phi = 0$ MV), where $\Delta E = 0.024$ MeV is the size of the bin containing $E = 0.511$ MeV. The total flux from the SSSBs $\mathcal{X}^{511} = F_{\rm tot}^{511}/F_{\rm Moon}^{511}$ can be calculated from eqs. (7)–(11). The SSSB albedo contribution to the 511 keV line flux within the Galactic bulge is $\sim 0.72 F_{\rm Moon}^{511}$, where we assumed that the FWHM of the bulge is $\sim 10°$ (Knödlseder et al. 2005), and $20°/360° \approx 0.06$, and we used the upper limit derived in Section 4. It gives $\sim 2 \times 10^{-5}$ photons cm^{-2} s^{-1}, which is about 2% of the total bulge emission as observed by the INTEGRAL $(1.05 \pm 0.06) \times 10^{-3}$ photons cm^{-2} s^{-1}

(Knödlseder et al. 2005). Since most of the INTEGRAL observing time was spent on observations of the Galactic bulge and a comparatively small fraction went into observing regions above and below the Galactic plane, it is not surprising that a diffuse band near the ecliptic (the SSSB albedo) has not been found so far. It is interesting that the OSSE map of the 511 keV line has a controversial feature, the so-called "annihilation fountain," above the Galactic bulge (Purcell et al. 1997) which, in fact, may be the asteroid albedo foreground instead. Note, that the γ-ray spectrometer on the NEAR-Shoemaker spacecraft made observations of the 511 keV line from 433 Eros (Evans et al. 2001) on the surface of Eros itself, however, it is hard to judge the absolute intensity of the line from the published data.

Our estimates of the fluxes assume that the mass and radius distributions are valid for the whole range of masses, which is not necessarily true. The number of small bodies may be larger or smaller than the extrapolation from the distribution of more massive bodies. We have also assumed spherical bodies. However, the smallest bodies are distinctly non-spherical which would make them somewhat brighter than we have estimated. Thus, our calculations underestimate the SSSB albedo emission.

The bodies that are smaller than the cutoff radius ($r_0 = 100$ cm for MBAs, 200 cm for Trojans, 400 cm for KBOs) will also contribute to the albedo flux. Because of their smaller size, only the initial stage of the CR cascade will develop, producing a harder albedo spectrum while its intensity will be reduced due to the partial conversion of energy of the primary CR particles into albedo γ-rays.

We emphasise that the detection of the γ-ray albedo from MBAs, KBOs, and other SSSB families directly probes the size distribution of these bodies below the detection limit of other methods, over considerably larger regions of the sky. The detectability of the γ-ray emission by these objects has implications for studies of the evolution of the solar and exo-solar planetary systems (Brown 2004), studies of CRs, and diffuse γ-rays. The GLAST Large Area Telescope (LAT)[6], to be launched by NASA in May 2008, will in just one year have an essentially uniform exposure over the entire sky a factor of 40 or more deeper than EGRET and will be free from sensitivity variations owing to ageing of consumables. This capability will permit detection of albedo γ-ray fluxes for SSSBs at even the Lunar flux level.

REFERENCES

Asphaug, E., & Benz, W. 1994, Nature, 370, 120
Babich, D., Blake, C. H., & Steinhardt, C. L. 2007, ApJ, 669, 1406
Backman, D. E., Dasgupta, A., & Stencel, R. E. 1995, ApJ, 450, L35
Baltz, E. A. et al. 2008, JCAP, submitted
Bergström, L., Ullio, P., & Buckley, J. H. 1998, APh, 9, 137
Bernstein, G. M., et al. 2004, AJ, 128, 1364
Binzel, R. P., Hanner, M. S., & Steel, D. I., 2003, Solar System Small Bodies, in Allen's Astrophysical Quantities, ed. Cox, A. N., p.315
Brown, M. E. 2001, AJ, 121, 2804
Brown, M. E. 2004, Physics Today, 57, 49
Cheng, A. F. 2004, Icarus, 169, 357
Dohnanyi, J. S. 1969, J. Geophys. Res., 74, 2531
Evans, L. G., et al. 2001, Meteoritics & Planetary Science, 36, 1639
Finkbeiner, D. P., & Weiner, N. 2007, Phys. Rev. D, 76, 083519
Gleeson, L. J. & Axford, W. I. 1968, ApJ, 154, 1011
Guessoum, N., Jean, P., & Gillard, W. 2005, A&A, 436, 171
Hartman, R. C., et al. 1999, ApJS, 123, 79
Hooper, D., Zaharijas, G., Finkbeiner, D. P., & Dobler, G. 2008, Phys. Rev. D, 77, 043511
Hunter, S. D., et al. 1997, ApJ, 481, 205
Ivezić, Ž., et al. 2001, AJ, 122, 2749
Jean, P., et al. 2006, A&A, 445, 579
Jedicke, R., & Metcalfe, T. S. 1998, Icarus, 131, 245
Jewitt, D. C., & Luu, J.-X. 1995, AJ, 109, 1867
Jewitt, D. C., et al. 2000, AJ, 120, 1140
Kenyon, S. J., & Bromley, B. C. 2004, AJ, 128, 1916
Knödlseder, J., et al. 2005, A&A, 441, 513
Krasinsky, G. A., Pitjeva, E. V., Vasilyev, M. V., & Yagudina, E. I. 2002, Icarus, 158, 98
Lacerda, P. & Jewitt, D. C. 2007, AJ, 133, 1393
Langner, U. W., Potgieter, M. S., Fichtner, H., & Borrmann, T. 2006, ApJ, 640, 1119
Luu, J.-X., & Jewitt, D. C. 2002, ARA&A, 40, 63
Mann, R. K., et al. 2007, AJ, 134, 1133
Marchis, F., et al. 2006, Nature, 439, 565
Moskalenko, I. V., & Porter, T. A. 2007, Proc. 30th Int. Cosmic Ray Conf. (Merida), in press; arXiv:0705.3856
Moskalenko, I. V., & Porter, T. A. 2007, ApJ, 670, 1467
Moskalenko, I. V., Porter, T. A., & Digel, S. W. 2006, ApJ, 652, L65
Moskalenko, I. V., Porter, T. A., Digel, S. W., Michelson, P. F., & Ormes, J. F. 2008, in Proc. 39th Lunar and Planetary Science Conference, #2280
Orlando, E., & Strong, A. W. 2007, Ap&SS, 309, 359
Orlando, E., Dirk, P., & Strong, A. W., 2007, in AIP Conf. Proc. 921, First Int. GLAST Symp., ed. Ritz, S. et al. (Melville:AIP), p.502
Prantzos, N. 2006, A&A, 449, 869
Ptuskin, V. S., Moskalenko, I. V., Jones, F. C., Strong, A. W., & Zirakashvili, V. N. 2006, ApJ, 642, 902
Purcell, W. R., et al. 1997, ApJ, 491, 725
Sheppard, S. S. 2005, Ph.D. Thesis, University of Hawaii
Sheppard, S. S., & Trujillo, C. A. 2006, Science, 313, 511
Solem, J. C. 1994, Nature, 370, 349
Sowards-Emmerd, D., Romani, R. W., & Michelson, P. F. 2003, ApJ, 590, 109
Sowards-Emmerd, D., Romani, R. W., Michelson, P. F., & Ulvestad, J. S. 2004, ApJ, 609, 564
Sreekumar, P., et. al. 1998, ApJ, 494, 523
Stone, E. C., et al. 2005, Science, 309, 2017
Stern, S. A. 2003, Nature, 424, 639
Strong, A. W., Moskalenko, I. V., & Reimer, O. 2004, ApJ, 613, 956
Takahashi, T., Mitsuda, K., & Kunieda, H., 2006, in SPIE Conf. Proc. 6266, Space Telescopes and Instrumentation II: Ultraviolet to Gamma Ray, ed. Turner, M. J. L. & Hasinger, G., p.62660D
Tancredi, G., Fernández, J. A., Rickman, H., & Licandro, J. 2006, Icarus, 182, 527
Tedesco, E. F., & Desert, F.-X. 2002, AJ, 123, 2070
Tedesco, E. F., Cellino, A., & Zappalá, V. 2005, AJ, 129, 2869
Thompson, D. J., Bertsch, D. L., Morris, D. J., & Mukherjee, R. 1997, J. Geophys. Res. A, 120, 14735
Toth, I., 2005, in IAU Symp. Proc. 229, Asteroids, Comets, Meteors, ed. Lazzaro, D. et al. (Cambridge: University Press), p.67
Weidenspointner, G., et al. 2006, A&A, 450, 1013
Wiegert, P., et al. 2007, AJ, 133, 1609
Yosihda, F., et al. 2003, Publ. Astr. Soc. Japan, 55, 701
Yoshida, F. & Nakamura, T. 2005, AJ, 130, 2900
Zaharijas, G., & Hooper, D. 2006, Phys. Rev. D, 103501